

## Stabilizing Predictive Visual Feedback Control for Fixed Camera Systems

TOSHIYUKI MURAO,<sup>1</sup> HIROYUKI KAWAI,<sup>2</sup> and MASAYUKI FUJITA<sup>3</sup>

<sup>1</sup>Advanced Institute of Industrial Technology, Japan

<sup>2</sup>Kanazawa Institute of Technology, Japan

<sup>3</sup>Tokyo Institute of Technology, Japan

### SUMMARY

This paper investigates vision-based robot control via a receding horizon control strategy for fixed camera systems, as stabilizing predictive visual feedback control. First, a visual motion robot error system with a fixed camera configuration is reconstructed in order to improve estimation performance. Next, stabilizing receding horizon control for three-dimensional visual feedback systems, which are highly nonlinear and relatively fast systems, is proposed. The stability of the receding horizon control scheme is guaranteed by using a terminal cost derived from an energy function of the visual motion robot error system. Furthermore, simulation and actual nonlinear experimental results are assessed with respect to stability and performance. © 2011 Wiley Periodicals, Inc. *Electron Comm Jpn*, 94(8): 1–11, 2011; Published online in Wiley Online Library (wileyonlinelibrary.com). DOI 10.1002/ecj.10357

**Key words:** visual feedback control; receding horizon control; passivity; stability; control Lyapunov function.

### 1. Introduction

Visual feedback control is a very flexible and effective method for the autonomous performance of various tasks for robotic systems [1, 2]. It is currently employed in a wide range of applications, including not only the fields of robotics and factory automation, but also automatic guidance of surgical instruments [3], control of an ultrasound probe held by a medical robot [4], injection of biological cells [5], and others. The authors have discussed passivity-based control for a moving target object in a three-dimensional (3D) workspace with a fixed camera configuration [6]. This control approach can be classified

as position-based visual feedback control, which is normally treated as both an estimation problem and a control problem. However, the control task has a negative effect on the estimation of relative rigid body motion in Ref. 6. Furthermore, the desired control performance cannot always be guaranteed explicitly, since the control method of Ref. 6 is not based on optimization.

Receding horizon control, also recognized as model predictive control, is a well-known control strategy in which the current control action is computed by solving a finite horizon optimal control problem on-line [7]. A large number of industrial applications using model predictive control can be found in chemical industries where the processes have relatively slow dynamics. For receding horizon control, many researchers have addressed the problem of stability guarantees. In contrast, for nonlinear and relatively fast systems such as in robotics, few implementations of receding horizon control have been reported. Jadbabaie and colleagues [8] showed that closed-loop stability is assured by the use of a terminal cost consisting of a control Lyapunov function. Furthermore, this result was applied to the Caltech Ducted Fan to perform aggressive maneuvers in Ref. 9. In Ref. 10, high effectiveness of stabilizing receding horizon control for a direct drive manipulator system is reported on the basis of experimental studies. However, visual feedback is not considered here.

Predictive control could be of significant benefit when used in conjunction with visual servoing. With the incorporation of visual information, the system could anticipate the target's future position and be waiting there to intercept it [11]. Ginhoux and colleagues [12] proposed a repetitive generalized predictive controller to cancel respiratory motions in robotized surgery. Lange and Hirzinger [13] presented a predictive visual tracking method using geometrical information to compute a desired path for high-speed industrial robots. Although good predictive control approaches using visual information are reported in those papers, stability is not addressed. In Ref. 14, the

authors proposed stabilizing receding horizon control for an eye-in-hand planar visual feedback system. However, the visual feedback system proposed in Ref. 14 is restricted to planar manipulators, and this method can treat only a desired position problem.

In this paper, we propose stabilizing receding horizon control for 3D visual feedback systems with a fixed camera configuration, which are highly nonlinear and relatively fast systems, as a method of predictive visual feedback control. First, a visual motion robot error system is reconstructed in order to improve estimation performance. Next, stabilizing receding horizon control for 3D visual feedback system using a control Lyapunov function is proposed. Since the proposed stabilizing visual feedback control law for the systems is based on receding horizon control theory, control performance should be improved relative to that of a nonoptimal control law. Compared with previous work [14], the proposed control law can treat not only position but also orientation, so that the range of possible application areas will undoubtedly be increased. The main idea is the use of a terminal cost derived from an energy function of the visual robot motion error system. Then, the control performance of the proposed control scheme is evaluated through simulation and experimental results.

The paper is organized as follows. In Section 2, we derive a visual motion robot error system for 3D fixed camera systems and discuss an energy function and a stabilizing control law. In Section 3, stabilizing receding horizon control for fixed camera systems using a control Lyapunov function is proposed. Section 4 describes simulation and experimental results that show the advantages of the proposed control laws, followed by conclusions in Section 5.

## 2. Visual Motion Robot Error System and Stabilizing Control Law

### 2.1 Vision camera model and estimation error system

A visual feedback system with a fixed camera configuration uses four coordinate frames, which consist of a world frame  $\Sigma_w$ , a hand (an end-effector of a manipulator) frame  $\Sigma_h$ , a camera frame  $\Sigma_c$ , and an object frame  $\Sigma_o$ , as shown in Fig. 1. Throughout this paper, we use the notation  $e^{\hat{\xi}\theta_{ij}} \in \mathcal{R}^{3 \times 3}$  to represent the rotation matrix of a frame  $\Sigma_j$  relative to a frame  $\Sigma_i$ .  $\xi_{ij} \in \mathcal{R}^3$  specifies the direction of rotation and  $\theta_{ij} \in \mathcal{R}$  is the angle of rotation. For simplicity we use  $\hat{\xi}\theta_{ij}$  to denote  $\hat{\xi}_{ij}\theta_{ij}$ . The notation “ $\wedge$ ” (wedge) is the skew-symmetric operator such that  $\hat{a}b = a \times b$  for the vector cross-product  $\times$  and any vector  $a, b \in \mathcal{R}^3$ , that is,  $\hat{a}$  is a  $3 \times 3$  skew-symmetric matrix. The notation “ $\vee$ ” (vee) denotes the inverse operator to “ $\wedge$ ,” that is,  $so(3) \rightarrow \mathcal{R}^3$ . Recall that

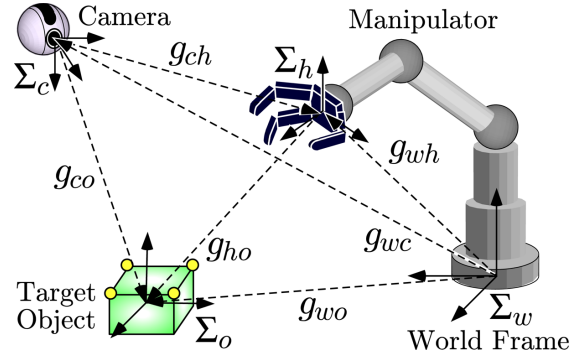


Fig. 1. Visual feedback system with a fixed camera configuration.

a skew-symmetric matrix corresponds to an axis of rotation (via the mapping  $a \mapsto \hat{a}$ ). We use the  $4 \times 4$  matrix

$$g_{ab} = \begin{bmatrix} e^{\hat{\xi}\theta_{ab}} & p_{ab} \\ 0 & 1 \end{bmatrix} \quad (1)$$

as the homogeneous representation of  $g_{ij} = (p_{ij}, e^{\hat{\xi}\theta_{ij}}) \in SE(3)$  describing the configuration of a frame  $\Sigma_j$  relative to a frame  $\Sigma_i$ . For example, the position and orientation in the object frame  $\Sigma_o$  relative to the hand frame  $\Sigma_h$  are expressed by  $g_{ho}$ .

The control objective is to bring the actual relative rigid body motion  $g_{ho}$  into agreement with a given constant reference one  $g_d$ . We now define a control error as follows:

$$g_{ec} := g_d^{-1} g_{ho} \quad (2)$$

which represents the error between the relative rigid body motion  $g_{ho}$  and the reference one  $g_d$ . We next define the error vector of the rotation matrix  $e^{\hat{\xi}\theta_{ei}}$  as  $e_R(e^{\hat{\xi}\theta_{ei}}) := \text{sk}(e^{\hat{\xi}\theta_{ei}})^\vee$ , where  $\text{sk}(e^{\hat{\xi}\theta_{ei}})$  denotes  $1/2(e^{\hat{\xi}\theta_{ei}} - e^{-\hat{\xi}\theta_{ei}})$ . Using this notation, the vector of the control error is given by  $e_c := [p_{ec}^T e_R(e^{\hat{\xi}\theta_{ec}})^T]^T$ .

The relative rigid body motion  $g_{ho}$  can be derived by using the composition rule for rigid body transformations [15] as follows:

$$g_{ho} = g_{ch}^{-1} g_{co} \quad (3)$$

Here,  $g_{ch} = g_{wc}^{-1} g_{wh}$  can be obtained directly, because the rigid body motions  $g_{wc}$  and  $g_{wh}$  are known from the structure of the system and the angles of the manipulator. We assume that the relative rigid body motion  $g_{ch}$  can be measured exactly in this paper. In contrast, the relative rigid body motion  $g_{co}$  can be derived as

$$g_{co} = g_{wc}^{-1} g_{wo} \quad (4)$$

The relative rigid body motion involves the velocity of each rigid body. We define the body velocity of the camera

relative to the world frame  $\Sigma_w$  as  $V_{wc}^b = [v_{wc}^T \omega_{wc}^T]^T$ , where  $v_{wc}$  and  $\omega_{wc}$  represent the velocity of the origin and the angular velocity from  $\Sigma_w$  to  $\Sigma_c$ , respectively [15]. Differentiating Eq. (4) with respect to time, the body velocity of the relative rigid body motion  $g_{co}$  can be written as follows (see Ref. 16):

$$V_{co}^b = -\text{Ad}_{(g_{co}^{-1})} V_{wc}^b + V_{wo}^b \quad (5)$$

where  $\text{Ad}_{(g_{ab})}$  is the adjoint transformation [15] associated with  $g_{ab}$  and  $V_{wo}^b$  is the body velocity of the target object relative to  $\Sigma_w$ .

In the case of a fixed camera configuration, that is,  $V_{wc}^b = 0$ , the body velocity  $V_{co}^b$  can be rewritten as

$$V_{co}^b = V_{wo}^b \quad (6)$$

In visual feedback control, the relative rigid body motion  $g_{co}$  cannot be utilized directly, but an image feature  $f \in \mathcal{R}^{2m}$  can be measured through a pinhole camera with perspective projection. Hence, we consider a nonlinear observer in order to estimate the relative rigid body motion  $g_{co}$  from the image feature  $f$ . Using the body velocity of the relative rigid body motion  $g_{co}$  (6), we choose estimates  $\bar{g}_{co} = (\bar{p}_{co}, e^{\hat{\xi}\theta_{co}})$  and  $\bar{V}_{co}^b$  of the relative rigid body motion and velocity, respectively, as

$$\bar{V}_{co}^b = u_e \quad (7)$$

The new input  $u_e$  is to be determined in order to drive the estimated values  $\bar{g}_{co}$  and  $\bar{V}_{co}^b$  to their actual values.

Here, we define the estimation error between the estimated value  $\bar{g}_{co}$  and the actual relative rigid body motion  $g_{co}$  as

$$g_{ee} := \bar{g}_{co}^{-1} g_{co} \quad (8)$$

Using the notation  $e_R(e^{\hat{\xi}\theta_{ei}}) = \text{sk}(e^{\hat{\xi}\theta_{ei}})^\vee$ , the vector of the estimation error is given by  $e_e := [p_{ee}^T e_R(e^{\hat{\xi}\theta_{ee}})^T]^T$ . Suppose that the attitude estimation error  $\theta_{ee}$  is small enough that we can let  $e^{\hat{\xi}\theta_{ee}} \approx I + \text{sk}(e^{\hat{\xi}\theta_{ee}})$ . Then using a first-order Taylor expansion approximation, the estimation error vector  $e_e$  can be obtained from the image feature  $f$  and the estimated value of the relative rigid body motion  $\bar{g}_{co}$  (i.e., the measurement and the estimate) as follows:

$$e_e = J^\dagger(\bar{g}_{co})(f - \bar{f}) \quad (9)$$

where  $\bar{f}$  is the estimated value of the image feature and  $J(\bar{g}_{co})$  is an image Jacobian-like matrix [16]. In the same way as Eq. (5), the estimation error system can be represented by

$$V_{ee}^b = -\text{Ad}_{(g_{ee}^{-1})} u_e + V_{wo}^b \quad (10)$$

## 2.2 Control error system

The objective of visual feedback control for fixed camera systems is to bring the actual relative rigid body

motion  $g_{ho}$  into agreement with a given constant reference  $g_d$ . In this subsection, let us consider a control error system in order to establish a visual robot motion error system.

In our previous work [6], using the estimated relative rigid body motion

$$\bar{g}_{ho} = g_{ch}^{-1} \bar{g}_{co} \quad (11)$$

we defined the control error as  $g_{ec} = \bar{g}_d^{-1} \bar{g}_{ho}$ . However, the estimation input  $u_e$  has directly affected not only estimation but also control; as a result, this leads to degraded estimation performance from the practical viewpoint. In order to remove the above negative effect in this paper, we define the control error as  $g_{ec} = \bar{g}_d^{-1} g_{ho}$  (2) between the actual relative rigid body motion  $g_{ho}$  and the desired one  $g_d$ .

Next, we derive the control error  $g_{ec}$  (2) without the nonmeasurable value  $g_{ho}$ . Using the estimation error matrix  $g_{ee} = \bar{g}_{co}^{-1} g_{co}$ , the control error can be transformed as

$$g_{ec} = g_d^{-1} g_{ho} = g_d^{-1} \bar{g}_{ho} \bar{g}_{ho}^{-1} g_{ho} = g_d^{-1} \bar{g}_{ho} g_{ee} \quad (12)$$

In Eq. (12),  $g_d$  and  $\bar{g}_{ho}$  are available information. While the estimation error vector  $e_e$  can be given by Eq. (9), the estimation error matrix  $g_{ee}$ , which is defined using the nonmeasurable value  $g_{co}$  as in Eq. (8), cannot be directly obtained. Focusing on the definition of the estimation error vector  $e_e$ , that is,  $e_e := [p_{ee}^T e_R(e^{\hat{\xi}\theta_{ee}})^T]^T$ , the position estimation error  $p_{ee}$  can be obtained directly from  $e_e$ . In the case of the rotation estimation error  $e^{\hat{\xi}\theta_{ee}}$ , if we assume that the region of the attitude estimation error is restricted to  $-\pi/2 \leq \theta_{ee} \leq \pi/2$ , then  $\xi\theta_{ee}$  can be obtained as follows:

$$\xi\theta_{ee} = \frac{\sin^{-1} \|e_R(e^{\hat{\xi}\theta_{ee}})\|}{\|e_R(e^{\hat{\xi}\theta_{ee}})\|} e_R(e^{\hat{\xi}\theta_{ee}}) \quad (13)$$

Therefore, it is possible to derive the control error  $g_{ec}$  using available information  $g_d$ ,  $\bar{g}_{ho}$ , and  $e_e$  by Eq. (12), since  $g_{ee}$  can be derived from  $e_e$  through  $\xi\theta_{ee}$  by using Eq. (1). A diagram showing the relationship between  $e_e$  and  $g_{ec}$  is given in Fig. 2. It should be noted that the assumption  $-\pi/2 \leq \theta_{ee} \leq \pi/2$  will not be a new constraint, since we have already made the assumption that the attitude estimation error  $\theta_{ee}$  is small enough in developing the estimation error vector  $e_e$  in Section 2.1.

Differentiating Eq. (2) with respect to time, the control error system can be represented as

$$V_{ec}^b = -\text{Ad}_{(g_{ec}^{-1})} \left( \text{Ad}_{(g_d^{-1})} V_{wh}^b \right) + V_{wo}^b \quad (14)$$

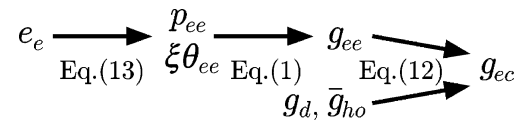


Fig. 2. Relationship diagram between  $e_e$  and  $g_{ec}$ .

### 2.3 Visual motion robot error system

The manipulator dynamics can be written as

$$M(q)\ddot{q} + C(q, \dot{q})\dot{q} + g(q) = \tau + \tau_d \quad (15)$$

where  $M(q) \in \mathcal{R}^{n \times n}$  is the inertia matrix,  $C(q, \dot{q}) \in \mathcal{R}^{n \times n}$  is the Coriolis matrix,  $g(q) \in \mathcal{R}^n$  is the gravity vector, and  $q$ ,  $\dot{q}$ , and  $\ddot{q}$  are the joint angle, velocity, and acceleration, respectively.  $\tau$  is the vector of the input torque, and  $\tau_d$  represents the disturbance input [17]. Since the manipulator dynamics is considered, the hand body velocity is given by  $V_{wh}^b = J_b(q)\dot{q}$ , where  $J_b(q)$  is the body manipulator Jacobian [15]. Let us define the error vector with respect to the joint velocity as  $\xi := \dot{q} - \dot{q}_d$ , where  $q_d$  represents the desired joint velocity.

Next, we propose control laws for the manipulator as

$$\begin{aligned} \tau = & M(q)\ddot{q}_d + C(q, \dot{q})\dot{q}_d + g(q) \\ & + J_b^T(q) \text{Ad}_{(g_d^{-1})}^T e_c + u_\xi \end{aligned} \quad (16)$$

where  $\ddot{q}_d$  represents the desired joint acceleration. The new input  $u_\xi$  is to be determined in order to reduce the joint velocity error  $\xi$ . Here, we design the reference of the joint velocity as  $\dot{q}_d := J_b^T(q)u_d$ , where  $u_d$  is the desired body velocity, obtained from the control error system part. Thus,  $V_{wh}^b$  in Eq. (14) should be replaced by  $u_d$ . Using Eqs. (10) and (14) to (16), a visual feedback error system with the manipulator dynamics (which we call the visual motion robot error system) can be derived as follows:

$$\begin{aligned} \begin{bmatrix} \dot{\xi} \\ V_{ec}^b \\ V_{ee}^b \end{bmatrix} &= \begin{bmatrix} -M^{-1}C\xi + M^{-1}J_b^T \text{Ad}_{(g_d^{-1})}^T e_c \\ -\text{Ad}_{(g_{ho}^{-1})} J_b \xi \\ 0 \end{bmatrix} \\ &+ \begin{bmatrix} M^{-1} & 0 & 0 \\ 0 & -\text{Ad}_{(g_{ec}^{-1})} & 0 \\ 0 & 0 & -\text{Ad}_{(g_{ee}^{-1})} \end{bmatrix} u + \begin{bmatrix} M^{-1} & 0 \\ 0 & I \\ 0 & I \end{bmatrix} w \end{aligned} \quad (17)$$

where  $u := [u_\xi^T (\text{Ad}_{(g_d^{-1})}^T u_d^T)^T]^T$  and  $w := [\tau_d^T (V_{wo}^b)^T]^T$ . We define the state of the visual motion robot error system as  $x := [\xi^T e_c^T e_e^T]^T$ , which consists of the joint velocity error  $\xi$ , the control error vector  $e_c$ , and the estimation error vector  $e_e$ . It should be noted that if  $x = 0$ , then the actual relative rigid body motion  $g_{ho}$  tends to the reference one  $g_d$ .

In the visual motion robot error system (17), the following important lemma concerning passivity between the input  $u$  and the output  $\nu$  holds.

**Lemma 1** If  $w = 0$ , then visual motion robot error system (17) satisfies

$$\int_0^T u^T \nu d\tau \geq -\beta_0, \quad \forall T > 0 \quad (18)$$

where  $\nu := Nx$ ,  $N := \text{diag}\{I, -I, -I\}$ , and  $\beta_0$  is a positive scalar.

Due to space limitations, the proof is only sketched. The proof can be completed by using the following energy function:

$$V = \frac{1}{2} \xi^T M \xi + E(g_{ec}) + E(g_{ee}) \quad (19)$$

where  $E(g_{ei}) := 1/2 \|p_{ei}\|^2 + \phi(e^{\xi \theta_{ei}})$ , and  $\phi(e^{\xi \theta_{ei}}) := 1/2 \text{tr}(I - e^{\xi \theta_{ei}})$  is an error function of the rotation matrix (see, e.g., Ref. 18).

### 2.4 Energy function and stabilizing control law

Based on the above passivity property of the visual motion robot error system, we now propose the following control input for the interconnected system:

$$\begin{aligned} u &= -K\nu = -KNx := u_k \\ K &:= \text{diag}\{K_\xi, K_c, K_e\} \end{aligned} \quad (20)$$

where  $K_\xi := \text{diag}\{k_{\xi_1}, \dots, k_{\xi_n}\}$  denotes the positive gain matrix for each joint axis of the manipulator.  $K_c := \text{diag}\{k_{c_1}, \dots, k_{c_6}\}$  and  $K_e := \text{diag}\{k_{e_1}, \dots, k_{e_6}\}$  are the positive gain matrices of the  $x$ ,  $y$ , and  $z$  axes of the translation and rotation for the control case and the estimation case, respectively. Considering the passivity of the visual motion robot error system shown in Lemma 1, the following theorem can be derived for stability.

**Theorem 1** If  $w = 0$ , then the equilibrium point  $x = 0$  for closed-loop system (17) and (20) is asymptotically stable.

*Proof* Differentiating Eq. (19) with respect to time and using control input (20), we obtain

$$\dot{V} = u^T \nu = -x^T N^T K N x \quad (21)$$

This completes the proof. (Q.E.D.)

Theorem 1 can be proved using the energy function (19) as a Lyapunov function. Here we compare proposed control law (20) with the previous one in Ref. 6. Block

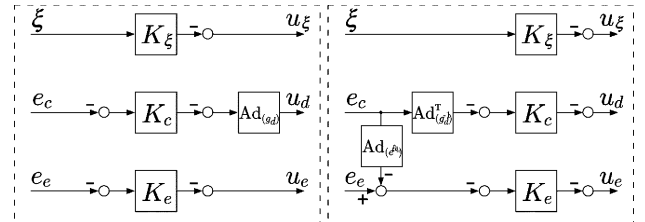


Fig. 3. Block diagram of part of the control law: left side, with proposed control law; right side, with previous control law [6].

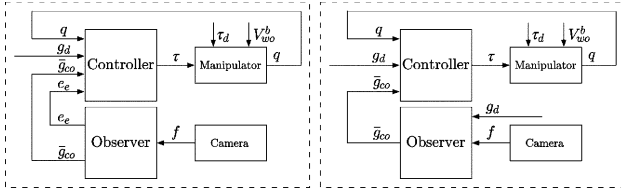


Fig. 4. Block diagram of the closed-loop system: left side, with proposed control law; right side, with previous control law [6].

diagrams of the part of the control law in the case of the proposed method and the previous one [6] are shown at the left and right sides of Fig. 3, respectively. In Ref. 6, the control error  $e_c$  has interfered with the input for the estimation  $u_e = K_e(e_e - \text{Ad}_{(e^{\xi_{ec}})} e_c)$ . In the sequel, the presence of  $e_c$  has negatively affected the estimation of the relative rigid body motion  $\bar{g}_{co}$ . On the other hand, with proposed visual feedback control law (20), the feedback inputs are separated by the error vectors, that is,  $u_\xi = -K_\xi \xi$ ,  $u_d = \text{Ad}_{(g_d)} K_c e_c$ , and  $u_e = K_e e_e$ . Thus, the proposed control law can overcome the problem of the above undesirable influence.

Similarly to Fig. 3, block diagrams of the closed-loop system in the case of the proposed method and the previous one [6] are shown on the left and right sides of Fig. 4, respectively. Differently from Ref. 6, the observer of the proposed system can be unaffected by the reference  $g_d$ , and thus it is clear that the estimation task is not directly impacted by the control task.

This is why the block matrix with respect to the input of the visual motion robot error system (17) is diagonal. It should be interpreted that the structure of the passivity-based visual feedback control can be separated into the estimation part and the control one in some way. This allows us to easily set the gains of control law (20) and the weights of the cost function (22) to (24) described below from a practical point of view.

However, visual feedback control law (20) is not based on optimization, and the desired control performance cannot be guaranteed explicitly. In the next section, stabilizing receding horizon control based on optimal control theory is proposed.

### 3. Stabilizing Predictive Visual Feedback Control

The objective of this section is to propose predictive visual feedback control based on optimal control theory. A camera can provide more information than the current derivation from a nominal position at the sample instant. This property can be exploited to predict the target's future position and improve control performance. As predictive

visual feedback control, we propose the stabilizing receding horizon control based on optimization in this paper.

#### 3.1 Control Lyapunov function for visual feedback systems

In this section, a finite horizon optimal control problem (FHOC) for visual motion robot error system (17) is considered. The FHOC for visual motion robot error system (17) at time  $t$  consists of minimization with respect to the input  $u(\tau, x(\tau))$ ,  $\tau \in [t, t+T]$  of the following cost function:

$$J(x_0, u, T) = \int_t^{t+T} l(x(\tau), u(\tau)) d\tau + F(x(t+T)) \quad (22)$$

$$l(x(t), u(t)) = q_\xi(t) \|\xi(t)\|^2 + E_{qc}(g_{ec}(t)) + E_{qe}(g_{ee}(t)) + u^T(t) R(t) u(t) \quad (23)$$

$$F(x) = \rho V(x) \quad (24)$$

$$q_\xi(t) \geq 0, q_{pi}(t) \geq 0, q_{Ri}(t) \geq 0, R(t) > 0, \rho > 0$$

where  $R(t)$  is a positive diagonal matrix, and  $E_{qi}(g_{ei}(t)) := q_{pi}(t) \|p_{ei}(t)\|^2 + q_{Ri}(t) \phi(e^{\xi_{ei}(t)})$  ( $i \in c, e$ ), with the state  $x(t) = x_0$ . The special property of cost function (22) to (24) is that the terminal cost is derived from the energy function of the visual motion robot error system. Furthermore, the rotation error-related part of the stage cost is derived from the error function  $\phi(e^{\xi_{ei}(t)})$  instead of the commonly used quadratic form  $\|e_R(e^{\xi_{ei}(t)})\|^2$ . For a given initial condition  $x_0$ , we denote this solution of the FHOC as  $u^*(\tau, x(\tau))$ ,  $\tau \in [t, t+T]$ . In receding horizon control, at each sampling time  $\delta$ , the resulting feedback control at state  $x_0$  is obtained by solving the FHOC and setting

$$u_{RH} := u^*(\delta, x_0) \quad (25)$$

A control Lyapunov function closely related to stability is defined as follows:

**Definition 1** [8] The control Lyapunov function  $S(x)$  is given by

$$\inf_u [\dot{S}(x) + l(x, u)] \leq 0 \quad (26)$$

where  $l(x, u)$  is a positive definite function. The following lemma concerning the control Lyapunov function is important in the proof of stabilizing receding horizon control.

**Lemma 2** Suppose that  $w = 0$ ,  $\|\theta_{ec}\| \leq \pi/2$ ,  $\|\theta_{ee}\| \leq \pi/2$ , and the design parameter  $\rho$  satisfies

$$\rho^2 I \geq 4QR \quad (27)$$

where  $Q := \text{diag}\{q_\xi I_n, q_{pc} I_3, q_{Rc} I_3, q_{pe} I_3, q_{Re} I_3\}$ . Then, the energy function  $\rho V(x)$  of visual motion robot error system (17) can be regarded as a control Lyapunov function.

*Proof* Using Eq. (21), which is the time derivative of  $V$  along the trajectory of system (17), the positive definite function  $l(x(t), u(t))$  (23) and the stabilizing control law  $u_k$  (20) with  $K = \rho/2R^{-1}$  for the system, Eq. (25) can be transformed into

$$\begin{aligned}
& \inf_u [\dot{S}(x) + l(x, u)] \\
&= \inf_u \left[ \rho \dot{V} + q_\xi \|\xi\|^2 + E_{qc}(g_{ec}) + E_{qe}(g_{ee}) + u^T R u \right] \\
&= \inf_u \left[ \rho x^T N^T u + q_\xi \|\xi\|^2 + E_{qc}(g_{ec}) + E_{qe}(g_{ee}) + u^T R u \right] \\
&= \inf_u \left[ \left( u + \frac{\rho}{2} R^{-1} N x \right)^T R \left( u + \frac{\rho}{2} R^{-1} N x \right) \right. \\
&\quad \left. - \frac{\rho^2}{4} x^T N^T R^{-1} N x + q_\xi \|\xi\|^2 + E_{qc}(g_{ec}) + E_{qe}(g_{ee}) \right] \\
&= -\frac{\rho^2}{4} x^T R^{-1} x + q_\xi \|\xi\|^2 + q_{pc} \|p_{ec}\|^2 \\
&\quad + q_{Rc} \phi(e^{\hat{\xi}\theta_{ec}}) + q_{pe} \|p_{ee}\|^2 + q_{Re} \phi(e^{\hat{\xi}\theta_{ee}}) \\
&\leq -\frac{\rho^2}{4} x^T R^{-1} x + q_\xi \|\xi\|^2 + q_{pc} \|p_{ec}\|^2 \\
&\quad + q_{Rc} \|e_R(e^{\hat{\xi}\theta_{ec}})\|^2 + q_{pe} \|p_{ee}\|^2 + q_{Re} \|e_R(e^{\hat{\xi}\theta_{ee}})\|^2 \\
&= -x^T \left( \frac{\rho^2}{4} R^{-1} - Q \right) x \tag{28}
\end{aligned}$$

where we have used the fact that  $\phi(e^{\hat{\xi}\theta_{ei}}) \leq \|e_R(e^{\hat{\xi}\theta_{ei}})\|^2$  for all  $\|\theta_{ei}\| \leq \pi/2$ . Therefore, the condition  $\inf_u [\dot{S}(x) + l(x, u)] \leq 0$  will be satisfied if the assumption  $\rho^2 I \geq 4QR$  is valid. (Q.E.D.)

Lemma 2 shows that the energy function  $\rho V(x)$  of the visual motion robot error system (17) can be regarded as a control Lyapunov function in the case of  $\rho^2 I \geq 4QR$ .

### 3.2 Stabilizing receding horizon control for visual feedback systems

We are now in a position to state the main result of this paper.

**Theorem 2** Consider the cost function (22) to (24) for the visual motion robot error system (17). Suppose that  $w = 0$ ,  $\|\theta_{ec}\| \leq \pi/2$ ,  $\|\theta_{ee}\| \leq \pi/2$ , and  $\rho^2 I \geq 4QR$ ; then the receding horizon control for the visual motion robot error system is asymptotically stabilizing.

*Proof* Our goal is to prove that  $J(x^*(t), u_{RH}, T)$ , which is the cost-to-go applying receding optimal control  $u_{RH}$ , will qualify as a Lyapunov function for the closed-loop system. We construct the following suboptimal control strategy for the time interval  $[t + \delta, t + T + \delta]$ :

$$\tilde{u} = \begin{cases} u^*(\tau) & \tau \in [t + \delta, t + T] \\ u_k(\tau) = -\frac{\rho}{2} R^{-1} N x, & \tau \in [t + T, t + T + \delta] \end{cases} \tag{29}$$

where  $u_k$  is stabilizing control law (20) with  $K = \rho/2R^{-1}$  for the visual motion robot error system. The associated cost is

$$\begin{aligned}
& J(x^*(t + \delta), \tilde{u}, T) \\
&= J(x^*(t), u^*, T) + \rho[V(x(t + T + \delta)) - V(x^*(t + T))] \\
&\quad - \int_t^{t+\delta} l(x^*(\tau), u^*) d\tau + \int_{t+T}^{t+T+\delta} l(x^*(\tau + T), u_k) d\tau \tag{30}
\end{aligned}$$

where  $x^*$  is the optimal state trajectory. This cost, which is an upper bound for  $J(x^*(t + \delta), u^*, T)$ , satisfies

$$\begin{aligned}
& J(x^*(t + \delta), u^*, T) - J(x^*(t), u^*, T) \\
&\leq \rho[V(x(t + T + \delta)) - V(x^*(t + T))] \\
&\quad - \int_t^{t+\delta} l(x^*(\tau), u^*) d\tau + \int_{t+T}^{t+T+\delta} l(x^*(\tau + T), u_k) d\tau \tag{31}
\end{aligned}$$

Using the positive definite function  $l(x(t), u(t))$  (23) and the stabilizing control law  $u_k$  (20) for the system, dividing both sides by  $\delta$ , and taking the limit as  $\delta \rightarrow 0$ , Eq. (31) can be transformed into

$$\begin{aligned}
& \lim_{\delta \rightarrow 0} \frac{J(x^*(t + \delta), u^*, T) - J(x^*(t), u^*, T)}{\delta} \\
&\leq -\frac{\rho^2}{4} x^{*T}(t + T) N^T R^{-1} N x^*(t + T) - x^{*T}(t) Q x^*(t) \\
&\quad - u^{*T} R u^* + q_\xi \|\xi^*(t + T)\|^2 + E_{qc}(g_{ec}^*(t + T)) \\
&\quad + E_{qe}(g_{ee}^*(t + T)) \\
&\leq -x^{*T}(t + T) \left( \frac{\rho^2}{4} R^{-1} - Q \right) x^*(t + T) \\
&\quad - x^{*T}(t) Q x^*(t) - u^{*T} R u^* \tag{32}
\end{aligned}$$

Considering that the control input during the first  $\delta$  is  $u_{RH} = u^*$ , by the assumption  $\rho^2 I \geq 4QR$ , the derivative of  $J(x^*(t), u_{RH}, T)$  is negative definite. Therefore, we have shown that  $J(x^*(t), u_{RH}, T)$  qualifies as a Lyapunov function and asymptotic stability is guaranteed. (Q.E.D.)

Theorem 2 guarantees the stability of the receding horizon control using a control Lyapunov function for the 3D visual motion robot error system (17), which is a highly nonlinear and relatively fast system. Since the stabilizing receding horizon control design is based on optimal control theory, the control performance should be improved compared to the passivity-based visual feedback control  $u_k$  (20), under the condition of adequate gain assignment in the cost function. It should be noted that the error function  $\phi(e^{\hat{\xi}\theta_{ei}})$  of the rotation matrix can be directly used in the stage cost (23). The assumption  $\rho^2 I \geq 4QR$  is very simple and it is quite easy to set the value of the design parameter  $\rho$ , by virtue of the fact that the matrix  $N$  is a block diagonal matrix, contrary to Ref. 6. Compared with the previous work [14], the main advantage of this approach is that the 3D visual feedback system is not restricted to a planar manipulator, and can treat not only the position but also the orientation. This allows us to extend the range of technological applications.

In this paper, the receding horizon controller predicts the states  $\xi$ ,  $g_{ec}$ , and  $g_{ee}$ , using the visual motion robot error

system (17) as the internal model. Considering that  $g_d$  is a given reference value, this implies that predictive visual feedback control anticipates the physical values  $\dot{q}$ ,  $g_{ho}$ , and  $\bar{g}_{co}$  from visual information. Also, it is interesting that receding horizon control is applied to the visual motion observer.

#### 4. Simulations and Experiments

In this section, the validity of the proposed control law is confirmed by simulation results in the case of a static target object and by experimental results in the case of a moving target object. The simulation and experimental results on a two-degree-of-freedom manipulator, as depicted in Fig. 5, are shown as a simple illustration of our proposed method, although it is valid for 3D visual feedback systems. The target object has four feature points.

##### 4.1 Simulation results

First, we present results for the stability analysis with the static target object. The simulation is carried out with the initial conditions  $q_1(0) = \pi/4$  rad,  $q_2(0) = \pi/12$  rad,  $p_{wc} = [0.4732 \ 0.1 \ 0.1]^T$  m,  $\xi_{\theta_{wc}} = [0 \ 0 \ 0]^T$  rad,  $p_{wo} = [0.3986 \ 0 \ -0.9]^T$  m,  $\xi_{\theta_{wo}} = [0 \ 0 \ -0.5087]^T$  rad. We use the references of the relative rigid body motion as constant values, that is,  $p_d = [0 \ 0 \ -0.9]^T$  m,  $\xi_{\theta_d} = [0 \ 0 \ 0]^T$  rad. The initial error condition  $x(0)$  is  $\xi(0) = [0 \ 0]^T$  rad/s,  $p_{ec}(0) = [-0.294 \ -0.293 \ 0]^T$  m,  $\xi_{\theta_{ec}}(0) = [0 \ 0 \ -1.556]^T$  rad,  $p_{ee}(0) = [0 \ -0.004 \ 0]^T$  m,  $\xi_{\theta_{ee}}(0) = [0 \ 0 \ -0.015]^T$  rad. The weights of cost function (22) to (24) were selected as  $q_\xi = 0.001$ ,  $q_{pc} = 0.1$ ,  $q_{Re} = 0.05$ ,  $q_{pe} = 0.3$ ,  $q_{Re} = 0.1$ , and  $R = \text{diag}\{0.1, 3.2, 0.7, 2, 2, 1, 1, 2, 0.3, 0.3, 0.3, 0.3, 0.3, 0.3\}$  and  $\rho = 1$  satisfy  $\rho^2 I \geq 4QR$ . To solve the real-time optimization problem, the

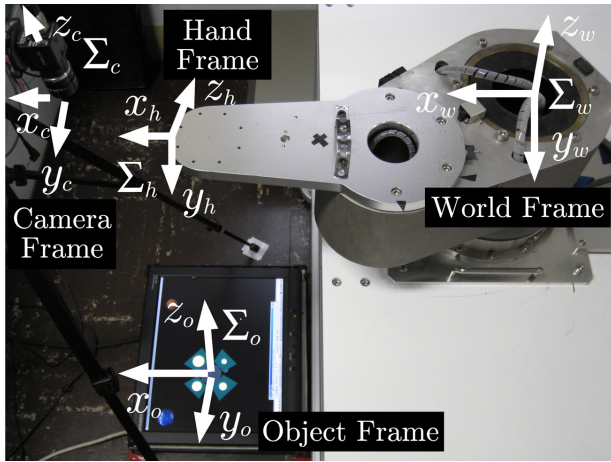


Fig. 5. Experimental arm and fixed camera.

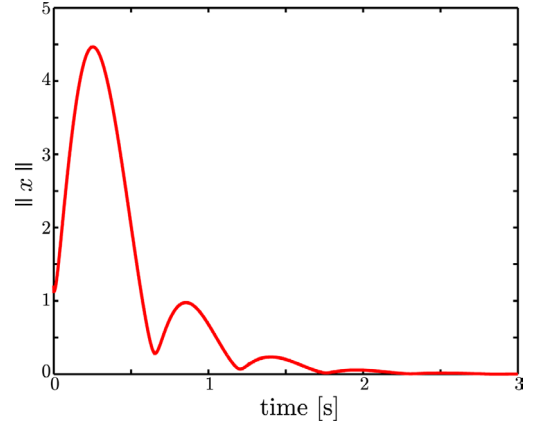


Fig. 6. Norm of the state.

C/GMRES software [19] is utilized. The control input with the receding horizon control is updated every 1 ms. It must be calculated by the receding horizon controller within that period. The horizon is selected as  $T = 0.02$  s. The norm of the state  $x$  applying the proposed control law is shown in Fig. 6. Asymptotic stability can be confirmed by steady-state performance.

Next, we compare the performance of the receding horizon control law  $u_{RH}$  (25) and the visual feedback control law  $u_k$  (20). The controller parameters for the passivity-based control law  $u_k$  (20) were empirically selected as  $K_\xi = \text{diag}\{10, 3\}$ ,  $K_c = \text{diag}\{2, 2, 1, 1, 1, 2\}$ ,  $K_e = \text{diag}\{1, 1, 1, 1, 1, 1\}$ . The aforementioned weights and these gains are selected in order not to exceed the limit of the input torque for the manipulator. Figure 7 shows the actual control error  $e_r := [p_{er}^T \ e_R^T(e^{\xi_{\theta_{er}}})^T]^T$ , which is the error vector

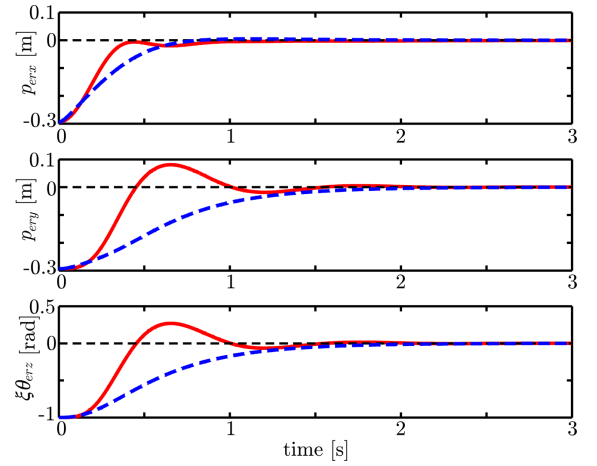


Fig. 7. Actual control error: solid, with predictive control law; dashed, with passivity-based control law.

between the actual  $g_{ho}$  and  $g_d$ . In Fig. 7, the solid lines represent the errors when applying the proposed stabilizing receding horizon control law  $u_{RH}$  (25), and the dashed lines represent those for the control law  $u_k$  (20). The rise time applying the receding horizon control is shorter than that for the passivity-based control law. These results suggest that the controller predicts the movement of the target object using the visual information, and as a result, the manipulator moves more aggressively. This validates one of the expected advantages of the stabilizing receding horizon control for visual feedback systems.

Next, the performance for the horizon length  $T$  and the design parameter value  $\rho$  is compared in terms of the integral cost in Table 1. The cost is calculated by the following function:

$$Cost = \int_0^I l(x(\tau), u(\tau)) d\tau \quad (33)$$

We set the integral interval  $I = 3$  in this simulation. Since the cost of the stabilizing receding horizon method is smaller than the passivity-based visual feedback control method (20) under the conditions of an adequate cost function, it can be easily verified that the control performance is improved. With increasing weight of the terminal cost from  $\rho = 1$  to  $\rho = 5$  the cost too increases. With higher terminal cost, the state value is reduced more strictly, using a large control input. In this simulation, since the weights of the control input are larger than those of the state, the cost increases. As the horizon length increases from  $T = 0.02$  to  $T = 0.5$ , the cost is reduced. In the case of  $T = 1$ , the calculation cannot be completed within one sampling interval, due to limited computing power.

## 4.2 Experimental results

In this subsection, we present experimental results for the case of a moving target object. The manipulator was controlled by a digital signal processor (DSP) from dSPACE Inc., which utilizes a powerPC 750 running at 480 MHz. The control problems were written in MATLAB and SIMULINK, and were implemented on the DSP using the

Table 1. Values of the cost function in simulation

Control Scheme	cost
Passivity based Control	3502
Receding Horizon Control ( $T = 0.02$ [s], $\rho = 1$ )	320
Receding Horizon Control ( $T = 0.02$ [s], $\rho = 2$ )	732
Receding Horizon Control ( $T = 0.02$ [s], $\rho = 5$ )	3152
Receding Horizon Control ( $T = 0.2$ [s], $\rho = 1$ )	301
Receding Horizon Control ( $T = 0.5$ [s], $\rho = 1$ )	256

Real-Time Workshop and dSPACE software, which includes ControlDesk, Real-Time Interface, and so on. We set up a Sony XC-HR57 camera which always kept all feature points of the target object in the field of view (see Fig. 5). The video signals were acquired by a PicPort-Stereo-H4D frame graver board and the HALCON image processing software. The sampling time of the controller and the frame rate provided by the camera were 1 ms and 60 fps, respectively. Hence, the image feature  $f$  was renewed every 16.7 ms. The control law  $\tau$  was interpolated every 5.6 ms using the most recent available data from the vision system. The difference between the sampling rate of the robot control and of the image grabbing system can be decreased by using commercially available cameras with superior performance.

The target object, projected on the liquid crystal display, had four feature points and moved for two time periods ( $0 \leq t < 0.85$  and  $2.15 \leq t < 3.4$ ), as depicted in Fig. 8. The experiment was carried out with the initial conditions  $q_1(0) = \pi/6$  rad,  $q_2(0) = -\pi/6$  rad,  $p_{wc} = [0.4732 \ 0.1 \ 0.1]^T$  m,  $\xi\theta_{wc} = [0 \ 0 \ 0]^T$  rad. We set the initial error condition  $x(0) = 0$ . The weights of the cost function (22) to (24) were selected as  $q_\xi = 0.1$ ,  $q_{pc} = 3$ ,  $q_{Rc} = 1$ ,  $q_{pe} = 30$ ,  $q_{Re} = 10$ , and  $R = \text{diag}\{0.1, 0.5, 0.05, 0.05, 0.05, 0.05, 0.05, 0.05, 0.008, 0.008, 0.008, 0.01, 0.01, 0.01\}$  and  $\rho = 1$  satisfied  $\rho^2 I \geq 4QR$ . The control input with receding horizon control was updated every 5.6 ms. The horizon was selected as  $T = 11.2$  ms.

Figure 9 shows the rigid body motion of the end-effector of the manipulator  $g_{wh}$ . The solid lines represent the rigid body motion  $g_{wh}$  applying the proposed stabilizing receding horizon control law, and the dashed lines denote the rigid body motion of the actual moving target object  $g_{wo}$ . In Fig. 9, it can be verified that the manipulator tracks the moving target object. Although a slight error remains in steady state because of the friction force with the manipulator, it decreases with increasing horizon length. Figure 10 illustrates the rigid body motion  $g_{wh}$  of the translation of  $y$  from 3.5 s to 3.6 s when the target object has just stopped. In Fig. 10, the actual trajectory is different from the reced-

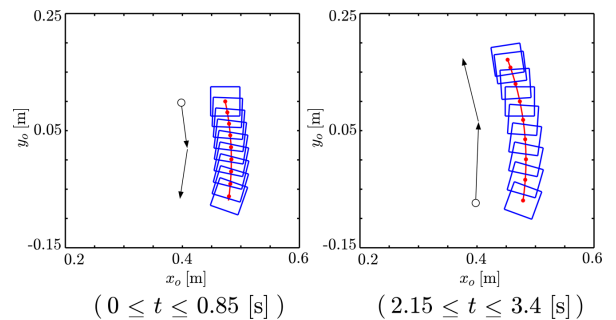


Fig. 8. Trajectory of the target object.

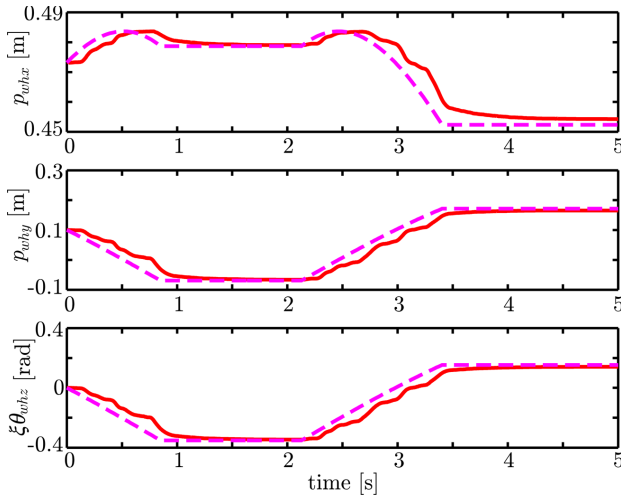


Fig. 9. Rigid body motion  $g_{wh}$ .

ing horizon reference values. This indicates that the manipulator can track the target object with re-prediction of the physical values  $\xi$ ,  $g_{ho}$ , and  $\bar{g}_{co}$ , even if its movement suddenly changes.

Finally, the performance for the horizon length  $T$  is compared in terms of the integral cost, calculated using Eq. (33) with  $I = 5$  in Table 2. Similarly to the simulation results, the cost is reduced as the horizon length increases from  $T = 0.0056$  to  $T = 0.056$ . For values greater than  $T = 0.056$ , the control law cannot be implemented due to limited computing power.

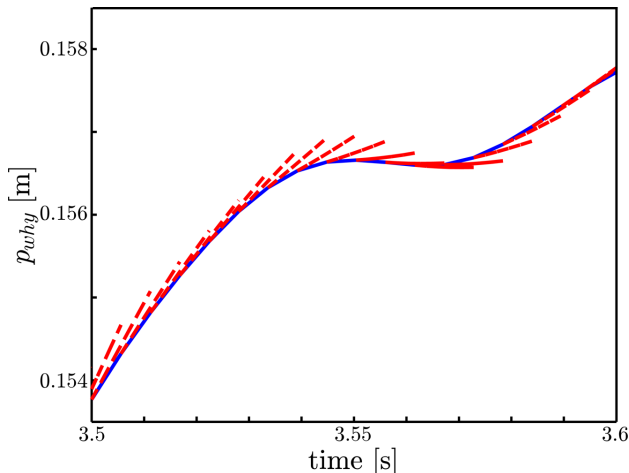


Fig. 10. Horizontal rigid body motion  $p_{why}$ : solid, with actual trajectory; dashed, with receding horizon reference trajectory.

Table 2. Values of the cost function in experiment

Control Scheme	cost
Passivity based Control	128.9
Receding Horizon Control ( $T = 0.0056$ [s], $\rho = 1$ )	88.8
Receding Horizon Control ( $T = 0.0112$ [s], $\rho = 1$ )	80.4
Receding Horizon Control ( $T = 0.028$ [s], $\rho = 1$ )	65.8
Receding Horizon Control ( $T = 0.056$ [s], $\rho = 1$ )	64.7

## 5. Conclusions

This paper proposes stabilizing receding horizon control for 3D fixed camera visual feedback systems, which are highly nonlinear and relatively fast systems, as a method of predictive visual feedback control. First, the visual motion robot error system is reconstructed in order to improve the estimation performance. Next, stabilizing receding horizon control for the visual feedback systems based on optimal control theory is designed. It is shown that the stability of the receding horizon control scheme is guaranteed by using the terminal cost derived from the energy function of the visual motion robot error system. It should be noted that the proposed stabilizing receding horizon control approach can be applied to visual feedback systems with a movable camera configuration [20]. In the simulation and experimental results, the control performance of the stabilizing receding horizon control is improved compared to that of passivity-based control.

## REFERENCES

1. Chaumette F, Hutchinson S. Visual servo control, Part I: Basic approaches. IEEE Robot Automation Mag 2006;13:82–90.
2. Chaumette F, Hutchinson S. Visual servo control, Part II: Advanced approaches. IEEE Robot Automation Mag 2007;14:109–117.
3. Omote K et al. Self-guided robotic camera control for laparoscopic surgery compared with human camera control. Am J Surg 1999;177:321–324.
4. Krupa A, Chaumette F. Control of an ultrasound probe by adaptive visual servoing. Proc of the 2005 IEEE/RSJ International Conference on Intelligent Robots and Systems, p 2007–2012.
5. Yu S, Nelson BJ. Autonomous injection of biological cells using visual servoing. In: Rus D, Singh S (editors). Experimental robotics VII. Springer-Verlag; 2001. p 169–178.
6. Kawai H, Murao T, Fujita M. Passivity-based control and estimation of dynamic visual feedback systems with a fixed camera. Proc of the 43rd IEEE Conference on Decision and Control, p 4022–4027, 2004.

7. Mayne DQ, Rawlings JB, Rao CV, Scokaert POM. Constrained model predictive control: Stability and optimality. *Automatica* 2000;36:789–814.
8. Jadbabaie A, Yu J, Hauser J. Unconstrained receding-horizon control of nonlinear systems. *IEEE Trans Automatic Control* 2001;46:776–783.
9. Milam MB, Franz R, Hauser JE, Murray RM. Receding horizon control of vectored thrust flight experiment. *IEE Proc Control Theory Appl* 2005; 152:340–348.
10. Kawai Y, Nakaso Y, Azuma T, Fujita M. Experiments on stabilizing receding horizon control of a direct drive manipulator. *Proc of the 16th IFAC World Congress on Automatic Control, Paper Code Tu-E04-TO/2*, 2005.
11. Hunt AE, Sanderson AC. Vision-based predictive robotic tracking of a moving target. Technical Report, Carnegie Mellon University, 1982.
12. Ginhoux R, Gangloff J, de Mathelin M, Soler L, Sanchez MMA, Marescaux J. Active filtering of physiological motion in robotized surgery using predictive control. *IEEE Trans Robot* 2005;21:67–79.
13. Lange F, Hirzinger G. Predictive visual tracking of lines by industrial robots. *Int J Robot Res* 2003; 22:889–903.
14. Fujita M, Murao T, Kawai Y, Nakaso Y. An experimental study of stabilizing receding horizon control of visual feedback system with planar manipulators. In: Findeisen R, Allgöwer F, Biegler L (editors). *Assessment and future directions of nonlinear model predictive control*. Springer-Verlag; 2007. p 573–580.
15. Murray R, Li Z, Sastry SS. *A mathematical introduction to robotic manipulation*. CRC Press; 1994.
16. Fujita M, Kawai H, Spong MW. Passivity-based dynamic visual feedback control for three dimensional target tracking: Stability and L2-gain performance analysis. *IEEE Trans Control Syst Technol* 2007;15:40–52.
17. Spong MW, Hutchinson S, Vidyasagar M. *Robot modeling and control*. John Wiley & Sons; 2006.
18. Bullo F, Lewis AD. *Geometric control of mechanical systems*. Springer-Verlag; 2004.
19. Ohtsuka T. A continuation/GMRES method for fast computation of nonlinear receding horizon control. *Automatica* 2004;40:563–574.
20. Murao T, Kawai H, Fujita M. Passivity-based control of dynamic visual feedback systems with movable camera configuration. *Electron Commun Japan* 2009;92:1–11.

#### AUTHORS (from left to right)



Toshiyuki Murao received a B.E. degree from the Department of Electrical and Computer Engineering, Kanazawa University, in 2003, an M.E. degree from the Division of Electronics and Computer Science, Kanazawa University, in 2005, and a D.Eng. degree from the Department of Mechanical and Control Engineering, Tokyo Institute of Technology, in 2008. Since 2006, he has been an assistant professor at the Advanced Institute of Industrial Technology. His research focuses on passivity-based visual feedback control of robot systems.

Hiroyuki Kawai received a B.S. degree from the Department of Electrical and Computer Engineering, Kanazawa University, in 1999, and M.S. and Ph.D. degrees from the Graduate School of Natural Science and Technology, Kanazawa University, in 2001 and 2004. From 2004 to 2005, he was a postdoctoral scholar at the Information Technology Research Center, Hosei University. In 2005, he joined Kanazawa Institute of Technology as an assistant professor. Since 2010, he has been an associate professor in the Department of Robotics. His research focuses on visual feedback control of robot systems and networked cellular vision systems. In particular, he is interested in passivity-based control. He received an IEEE Transactions on Control Systems Technology Outstanding Paper Award from the IEEE Control Systems Society (CSS) in 2008.

## AUTHORS (continued)



Masayuki Fujita is a professor in the Department of Mechanical and Control Engineering, Tokyo Institute of Technology. He received a D.Eng. degree in electrical engineering from Waseda University in 1987. Prior to his appointment at Tokyo Institute of Technology, he held faculty appointments at Kanazawa University and the Japan Advanced Institute of Science and Technology. He also held a visiting position at the Technical University of Munich, Germany. His research interests include passivity-based visual feedback, cooperative control, and robust control with its industrial applications. He has served as General Chair of the 2010 IEEE Multi-Conference on Systems and Control. He is currently a Vice President of the IEEE CSS and a member of the IEEE CSS Board of Governors, and was a Director of SICE. He has served/been serving as an associate editor for *IEEE Transactions on Automatic Control*, *IEEE Transactions on Control Systems Technology*, *Automatica*, and the *Asian Journal of Control*, and as an Editor for the *SICE Journal of Control, Measurement, and System Integration*. He is a recipient of a 2008 IEEE Transactions on Control Systems Technology Outstanding Paper Award. He has also received Outstanding Paper Awards from the SICE and the ISCIE, and a 2010 SICE Education Award.